

Electrochemical Detection of Nitroenergetics for Long Term Monitoring

B.J. White,¹ B.J. Melde,¹ R.L. Siefert,² and M. Nasir³

¹Center for Bio/Molecular Science and Engineering

²U.S. Naval Academy

³Lawrence Technological University

Monitoring Contaminated Sites: U.S. Department of Defense activities related to ordnance manufacture, storage, disposal, and training have resulted in nitroenergetic contamination at a number of military installations. Monitoring and remediation of these sites is costly, leading to significant interest in more effective and efficient methods. Traditionally, monitoring is accomplished through collection of samples that are subsequently returned to a laboratory for analysis. This requires careful handling to protect against erroneous results and imposes a significant logistical burden. In situ monitoring offers flexibility in sampling frequency, improved information on system dynamics, and elimination of handling considerations. The use of electrochemical sensors offers the benefits of small size, low power requirements, and low cost to portable applications. Current commercially available sensors, however, do not provide sufficient sensitivity or selectivity to replace traditional methods.

Preconcentration for Improved Performance: Preconcentration by solid-phase extraction (SPE) involves adsorbing targets onto a solid support followed by desorption using a solvent. The result is more target in a smaller volume. Selective and semiselective adsorption can also help to eliminate nontarget compounds from the concentrated sample. Our effort is focused on developing the materials and systems necessary for inline preconcentration prior to analysis by electrochemical methods. The approach is intended to improve the detection limits for such a system and to eliminate potential inference by the sample matrix. The SPE sorbents developed are porous organosilicates providing semiselective binding of 2,4,6-trinitrotoluene (TNT), RDX, HMX, and dinitrotoluenes (DNT). These materials preconcentrate targets and eliminate nontarget contaminants as demonstrated by high performance liquid chromatography (HPLC) based studies.^{1,2} They show improved target retention and selectivity over commercially available SPE sorbents. The materials can be used repeatedly over periods of months with no degradation in performance and are applicable across a wide range of temperatures and chemical conditions.

The Inline System: The inline system is intended to provide sample collection, preconcentration, and

elution prior to analysis by an electrochemical detector (Fig. 1). Samples are pulled through a filter stack to eliminate particulates (size exclusion) using a peristaltic pump that also pushes the sample through the sorbent column. Once target is adsorbed, the precolumn valve is switched, and eluent is pushed through the column. The desorbed targets are then directed to the electrochemical detector after mixing with electrolyte solution. A single sorbent column was used for evaluation of more than 220 samples including deionized, ground, and surface water and soil extracts. The total time for processing using the prototype system (30 mL sample volume) was 45 min. During analysis of this sample series, it was necessary to replace the silicon tubing used in the peristaltic pump three times. Continued use of a single tubing set resulted in damage and eventual rupture of the tubing after 100 to 150 h of system use.

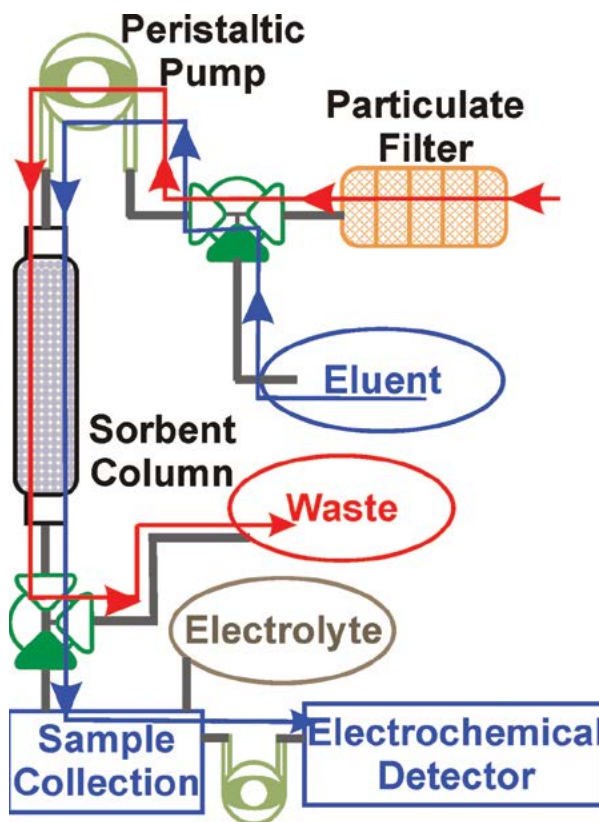


FIGURE 1

Preconcentration system. Shown here is a schematic of the prototype system developed by NRL. The red line indicates flow of the water sample through the system, entering at the particulate filter and exiting to waste. The blue line indicates the flow of eluent through the system, carrying concentrated target to the electrochemical detector.

System Performance: A PalmSens handheld potentiostat (PalmSens, Utrecht, The Netherlands) was selected for electrochemical (EC) measurements based on square wave voltammetry. Calibration of the EC

sensor indicated limits of detection at 250 ppb for TNT and 350 ppb for DNT. While RDX is of particular interest for in situ monitoring, the target does not lend itself to detection using commercially available components.³ Having established the performance of the EC system, the impact of preconcentration prior to EC analysis was evaluated. Samples in deionized water between 20 and 250 ppb were considered (30 mL). Samples of lower concentration were evaluated using larger sample volumes (300 mL). In the case of TNT, the variability between HPLC determined values and EC determined values is 26% on average with 23% for DNT data set. Evaluation of samples in ground water (Fig. 2(b)) indicated similar results for TNT and greater variation for DNT (40%), likely due to the analysis method utilized.

TNT detection using this method is encouraging. Discrimination of TNT from DNT and RDX was achieved without difficulty in blind sample analysis (Fig. 2(c)). Nitroglycerin presence was interpreted as low TNT concentrations by an operator with no knowledge of sample composition. While samples in ground water could not be analyzed by the EC system, use of inline preconcentration provided elimination of the interferents as well as enhanced target concentrations, resulting in performance similar to that in deionized water. Depending on the volume of sample used for preconcentration, detection limits for the electrochemical sensor could be reduced by up to two orders of magnitude (250 ppb to less than 3 ppb). While the approach was less successful for DNT, the study thoroughly demonstrates the potential of such a system. The use of modified electrodes, not currently commercially available, provides the potential for detection of additional targets, such as DNT and RDX.³

Acknowledgments: The authors would like to thank I.A. Leska, J.R. Taft, M.H. Moore, and A.P. Malanoski for their contributions to this effort. This research was sponsored by the Strategic Environmental Research and Development Program (SERDP, ER-1604) and conducted at the Naval Research Laboratory, Washington, DC.

[Sponsored by SERDP]

References

- B.J. Johnson, B.J. Melde, P.T. Charles, M.A. Dinderman, A.P. Malanoski, I.A. Leska, and S.A. Qadri, "Macroporous Silica for Concentration of Nitroenergetic Targets," *Talanta* **81**, 1454–60 (2010).
- B.J. Johnson, B.J. Melde, I.A. Leska, P.T. Charles, and A.D. Hewitt, "Solid-Phase Extraction Using Hierarchical Organosilicates for Enhanced Detection of Nitroenergetic Targets," *J. Environ. Monitor.* **13**, 1404–9 (2011).
- S.Y. Ly, D.H. Kim, and M.H. Kim, "Square-Wave Cathodic Stripping Voltammetric Analysis of RDX Using Mercury-Film Plated Glassy Carbon Electrode," *Talanta* **58**, 919–926 (2002).

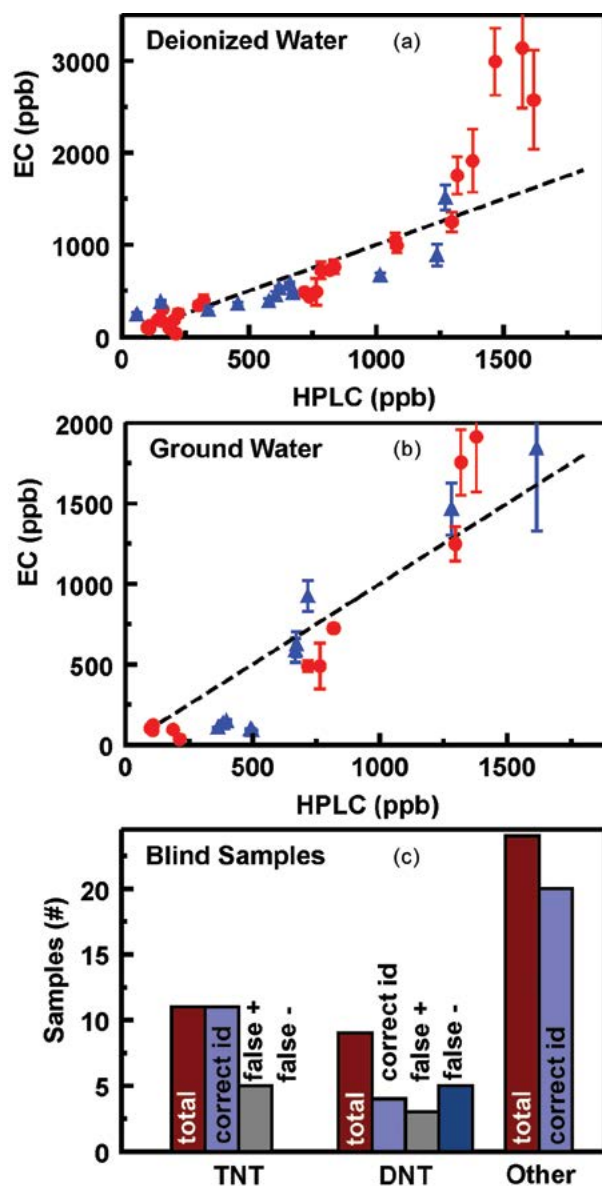


FIGURE 2 Preconcentration of targets. In (a) and (b), points here represent the results for quantification of targets from deionized water (a) and ground water (b) using the prototype system with analysis by HPLC (x-axis) and EC (y-axis): TNT (red) and DNT (blue). The line indicates the expected results based on HPLC analysis of the spiked samples. Error bars indicate the standard deviation in the measurements; where not visible, they are within the size of the symbol. Shown in (c) are results of blind sample analysis. The bars shown here indicate the total number of samples containing either TNT or DNT and the associated number of correct target identifications. Also shown are the number of false positive and negative responses. The third category of samples includes those with no target and those with targets not expected to be detected (RDX, nitroglycerin).

Remote Sensing Signatures of Breaking Waves from Multi-Instrument Field Experiment on FLIP

M.D. Anguelova,¹ D.J. Dowgiallo,¹ G.B. Smith,¹
S.L. Means,² I.B. Savelyev,¹ G.M. Frick,¹ C.M. Snow,¹
J.A. Schindall,² and J.P. Bobak¹

¹Remote Sensing Division

²Acoustics Division

Introduction: Oceanic whitecaps are the surface expression of breaking wind waves in the ocean. Whitecap fraction W , defined as the fraction of a unit surface covered with sea foam, quantifies wave breaking and is thus a suitable forcing variable for parameterizing and predicting air-sea interaction processes associated with breaking waves. Whitecaps in different lifetime stages have markedly different properties. Active whitecaps, formed at the moment of active breaking, are thick, comprise a wide range of bubble sizes, move along with the wave crest, and cover less surface area. Residual whitecaps, comprising decaying foam, are thinner, remain motionless behind the wave that has created them, and spread over a larger area. Total W (active plus residual whitecaps) is a useful predictor of bubble-mediated sea spray production and heat exchange.¹ More dynamical air-sea processes are better represented by active whitecap fraction W_A , e.g., production of spume droplets (important for tropical storms intensification), momentum flux, turbulent mixing, gas exchange, and generation of ambient noise in the ocean.²

A database of W from satellite-measured brightness temperature T_B of the ocean surface at microwave frequencies has been developed within the framework of the WindSat mission at NRL.³ This database is useful for studying and parameterizing W variability. However, to make this database useful for dynamic processes, it is necessary to find a way to extract W_A from W . We pursue separation of W_A from W both theoretically and experimentally. The physical basis for the experimental approach is that there are distinct signature differences between active and residual whitecaps at infrared (IR) wavelengths.⁴ To this end, we conducted a multi-instrument field campaign to collect data useful for identifying the signatures of breaking waves and whitecaps at different electromagnetic wavelengths, from visible, to IR, to microwave.

Field Campaign: We collected data from April 22 to 30, 2012, on the Floating Instrument Platform (FLIP) drifting along the coast of California from Monterey Bay south. FLIP is a unique vessel (<http://www-mpl.ucsd.edu/resources/flip.intro.html>) that provides a stable research platform for data collection on three

booms (port, starboard, and face). FLIP is towed to its operating area in a horizontal position and, through ballast changes, is “flipped” to a vertical position to become a stable spar buoy with a draft of 300 ft (Fig. 3(a)). The diameter of the hull tapers with depth, and this makes FLIP less responsive to wave motion.

Variations of ocean surface brightness temperature, T_B , caused by breaking waves and whitecaps were measured with microwave radiometers at frequencies of 10 and 37 GHz, vertical and horizontal (VH) polarizations. The radiometers, mounted on the port boom within a weather casing (Fig. 3(b)), looked at the ocean surface at an angle of 45°. The beamwidths of the 10- and 37-GHz horns are approximately 6°, giving an approximate footprint of 1.8 m in diameter for each instrument. The infrared imager used during this exercise was a Merlin-Mid (Indigo Systems, a division of FLIR). This system is sensitive to radiation in the 3 to 5 μm band (mid-wave infrared) and has a noise equivalent ΔT of approximately 0.017 K. Imagery was typically collected at a sampling rate of 10 Hz. The IR camera was mounted on top of the radiometers (Fig. 3(b)) to ensure the radiometer footprints fell within the

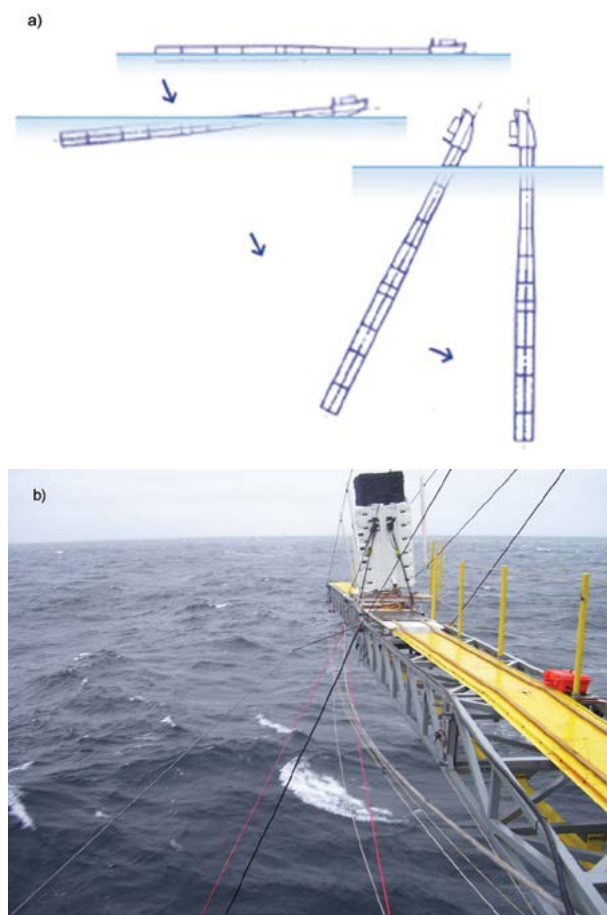


FIGURE 3
Research platform FLIP: a) controlled sinking to vertical position; b) instrumentation deployed on port boom.

16 × 12 m² field of view (FOV) of the IR camera. Three video cameras, positioned in different places, recorded visible images of whitecaps.

An acoustic vertical line array (VLA) provided data for the bubble-generated noise beneath breaking waves. The VLA was suspended between the face and port booms of FLIP. The array consisted of three nested apertures with hydrophones spaced at 1.25, 0.625, and 0.3125 m, yielding design frequencies of 600, 1200, and 2400 Hz, respectively. The VLA was deployed at a depth such that the upward endfire beam would isolate acoustic signatures from individual breaking waves, excluding FLIP-generated noise at all but the lowest frequencies.

The aerosol size distribution was measured with two instruments. A Particle Measuring Systems CSASP-100-HV, suspended from the starboard boom, measured aerosol from 0.25 to 23.5 μm radius. The NRL Differential Mobility Analyzer measured ducted and dried aerosol between 6 and 400 nm radii.

Various auxiliary data such as wind speed, air temperature, humidity, wave field, and water temperature profile characterize the experimental conditions. The conditions encountered ranged from wind speed of 2.8 to about 18 m s⁻¹, and significant wave height from 1 to ~5 m (Fig. 4).

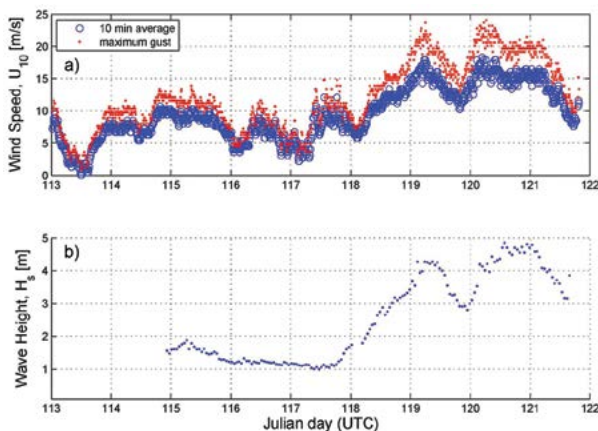


FIGURE 4
Experimental conditions: a) wind speed; b) significant wave height.

Data Collected: Figure 5 shows typical data collected from each instrument. A bright whitecap seen in the visible image (Fig. 5(a)) is identified by dark streaks at IR wavelengths (Fig. 5(b)). Spikes in T_b at 10 GHz, seen simultaneously in both H and V polarizations, mark whitecap signatures at microwave wavelengths (Fig. 5(c)). The observed increased noise level (in dB) is the whitecap acoustic signature (Fig. 5(d)).

IR images will help us identify active and residual foam as warm and cold patches, respectively. Matching these signals in time with radiometric, acoustic,

and aerosol data will help us identify the signatures of the two life stages at other wavelengths. We will then establish criteria for active vs residual separation for each type of data. Correlating radiometric, acoustic, and aerosol signature characteristics with each other, as well as with meteorological and oceanographic data, will yield empirical relationships useful for predicting breaking wave and whitecaps with observations from various sensors.

The impact of our findings will be the improvement of the current accuracy of predicting air-sea fluxes at the air-sea interface. More accurate air-sea fluxes will, in turn, reduce the uncertainty of weather forecasting, tropical cyclone intensification, wave forecasting, and climate prediction.

Acknowledgments: This work was sponsored by the Office of Naval Research (ONR), NRL Program element 61153N WU 4500. We highly appreciate the funding support for our use of FLIP by Robert Schnoor via the Naval Research Facilities Program at ONR, and by Dr. Joan Gardner and Dr. Edward Franchi via the NRL Platform Support Program. Captain William Gaines, FLIP program manager at Marine Physics Laboratory (MPL) at Scripps Institution of Oceanography, was indispensable in organizing the field campaign. We appreciate Tom Golfinos, Officer-in-Charge for FLIP, and crew members Johnny, Dave, Frank, and Jerry for their hard work, endurance, and camaraderie. We would also like to thank George Trekas and his colleagues at the MPL Machine Shop for their expertise and skills in devising the instrument deployment on the FLIP booms.

[Sponsored by ONR]

References

- ¹ G. de Leeuw, E. Andreas, M.D. Anguelova, C. Fairall, E. Lewis, C. O'Dowd, M. Schulz, and S. Schwartz, "Production Flux of Sea-Spray Aerosol," *Rev. Geophys.* **49** (2011).
- ² W.K. Melville, "The Role of Surface-Wave Breaking in Air-Sea Interaction," *Annu. Rev. Fluid Mech.* **28**, 279–321 (1996).
- ³ P.W. Gaiser, K.M. St Germain, E.M. Twarog, G.A. Poe, W. Purdy, D. Richardson, W. Grossman, W.L. Jones, D. Spencer, G. Golba, J. Cleveland, L. Choy, R.M. Bevilacqua, and P.S. Chang, "The WindSat Spaceborne Polarimetric Microwave Radiometer: Sensor Description and Early Orbit Performance," *IEEE Trans. Geosci. Rem. Sens.* **42**, 2347–2361 (2004).
- ⁴ G.O. Marmorino and G.B. Smith, "Bright and Dark Ocean Whitecaps Observed in the Infrared," *Geophys. Res. Lett.* **32**, L11604 (2005).

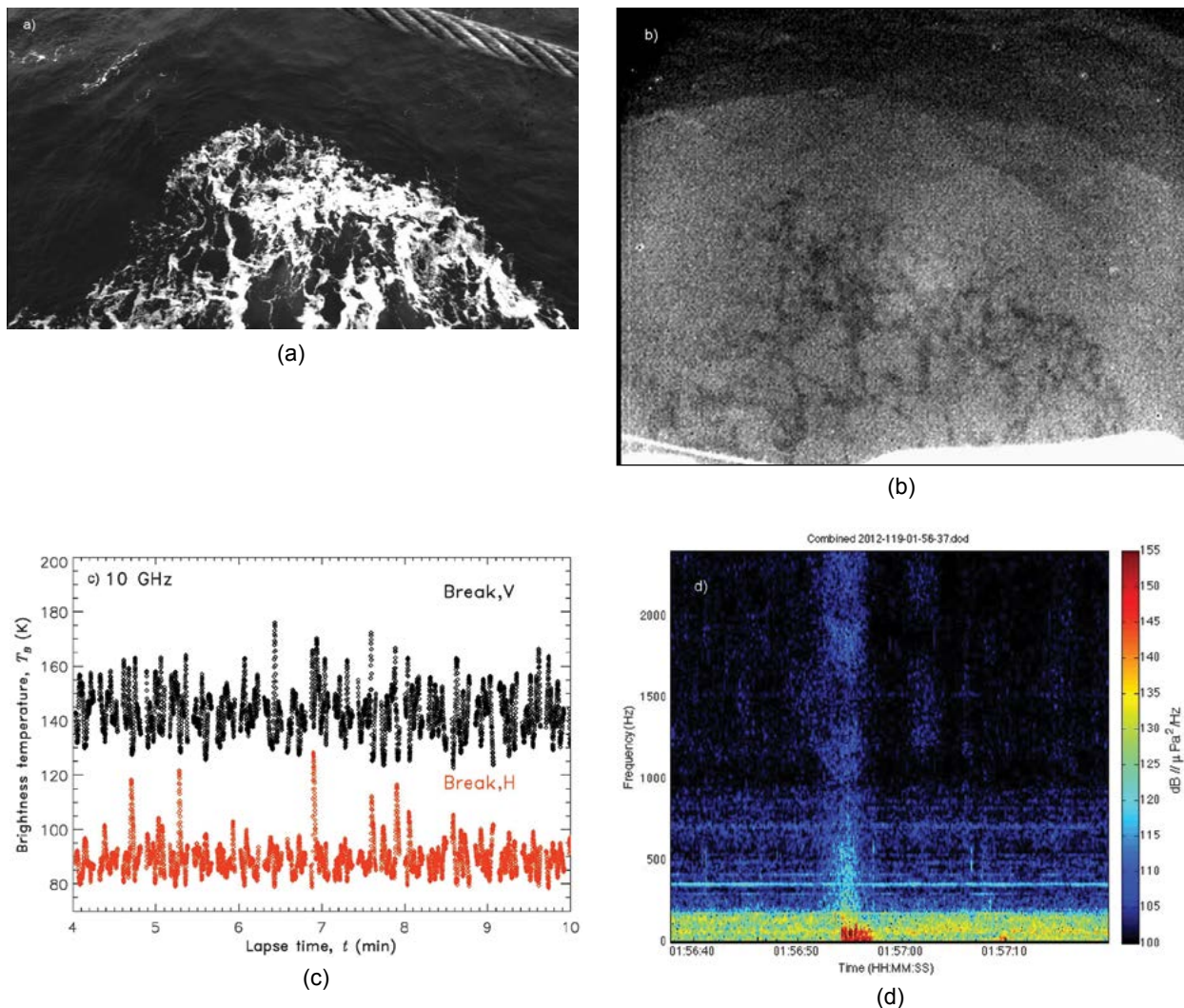


FIGURE 5 Breaking wave signatures at different wavelengths: a) visible; b) infrared; c) microwave (10 GHz); and d) acoustic.

Surprising Discoveries in Reflectance Properties of Complex Granular Sediments

A. Abelev¹ and C.M. Bachmann²

¹Marine Geosciences Division

²Remote Sensing Division

Introduction and Background: Terrestrial remote sensing applications are abundant in various fields of science and technology, applicable and currently in high demand in both the civilian and the military domains. One of the main goals of these applications is determination of the nature, properties, and composition of soils — natural and engineered alike. Multi- and hyperspectral measurements represent one of the main and quickly growing sectors of remote sensing, with

sensors deployed near the ground, in the air, and in Earth's orbit. The characteristic nature of the way that these sensors are used involves a phase angle dependence of measurements (angle between the line of sensor sight and the illumination line of the sun). This influence is expressed in models via a bidirectional reflectance distribution function (BRDF). Characteristics such as texture, grain-size distribution, and mineralogical composition are phase-angle dependent and represent the first level of complexity in characterizing soil properties and behaviors. These properties are features of the very surface of the soil, visible on the scale of the wavelength of a hyperspectral instrument spectrum, typically including some parts or all of the visible (VIS), near infrared (NIR), and shortwave IR (SWIR) ranges (0.4 to 2.5 μm). Additionally, some of the bulk properties of the soils are of great interest to the end-user and include, e.g., bulk density and porosity. Describing these properties involves the mechani-

cal characteristics of soils (and granular materials in particular), which rely on volume properties and are much harder to determine from overhead sensors. One of these volume properties is the relative density – i.e., the degree of grain packing in the range between the loosest (minimum density) and the densest (maximum) arrangement of grains a material can attain in the natural environment. The knowledge of this critical property leads to much higher levels of utility, up to and including certain soil strength parameters, such as a friction angle of the granular media.

Current state-of-the-art radiative transfer theories for granular media of a single constituent predicts increased reflectance with increased degree of material packing,^{1,2} or relative density. These theories have been validated using a variety of models and confirmed by experiments on assemblies of particles of the same mineralogical composition. These theories have also been applied to coastal soils, where some of the underlying principles may not hold true due to the typically very complex and heterogeneous mineralogical composition. In this work, we explore the directional reflectance dependence of a natural complex beach sand on its relative density. As a result of our experimental investigation,³ we uncovered some surprising effects that demonstrate a clear dependence of the reflectance on the relative density (or packing) of the material, but in exactly opposite form from that predicted by all current theories. We explain that the origin of these observations lies in the mineral complexity of the beach material.

Experimental Investigation and Discussion: The sand that was recovered from the Virginia Coast Reserve (VCR) during an experiment⁴ was reconstituted in the laboratory using an air-pluviation method⁵ that more closely represents the natural Aeolian formation processes than do the artificial compaction modes. The method involves sand air-pluviation through a series of sieves that serve as flow diffusers, dispensing from a calibrated height and at a given flow rate into a special mold. Various rates of deposition (and drop heights) result in a wide range of densities, from the very loose (for quick flows) to the very dense (for slow pours). The experimental apparatus for studying directional dependence of the reflectance was built (Fig. 6) and includes an Analytical Spectral Devices (ASD) spectrometer, recording radiance in the spectral range between 0.35 and 2.5 μm , with an 8° fore-optic, and an ASD lamp (as a light source), both mounted on booms and rotational stages with independent accurate positioning. This design allows for an exploration of reflectance values for a wide range of phase angles from 7° to 50° in the principal scattering plane. Select results from different ranges in the spectrum (VIS, NIR, SWIR) are

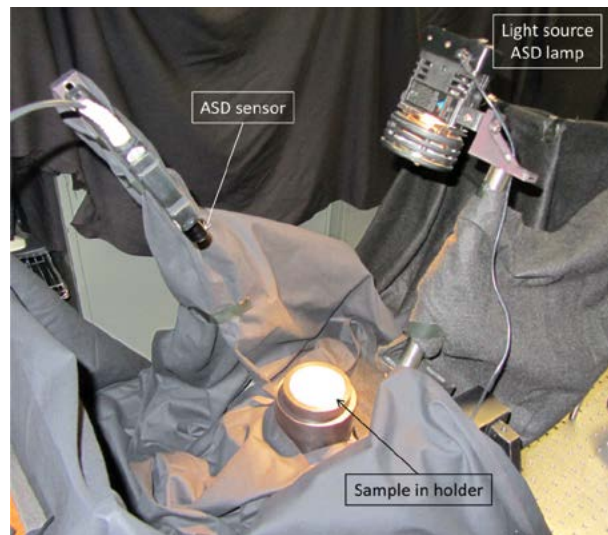


FIGURE 6 Experimental setup showing an ASD hyperspectral sensor (0.35 to 2.5 μm) with an 8° fore-optic and a light source, each mounted on a boom attached to a rotational stage with precise angular positioning. Reconstituted sample is shown in a Delrin holder. Black cloth shrouding covers reflective metal parts to minimize extraneous interference to measured sand surface reflectance.

shown in Fig. 7. These wavelengths were chosen at a few notable absorption features of the spectral curves. Additionally, surface images of the low and high density sand samples, taken at 4× magnification through a microscope, are shown as an inset in Fig. 7. The reflectance values for all phase angles plotted increase from high to low relative density, opposite of what might be expected and predicted with any of the current single-constituent theories. The source of this unexpected change lies in the complex mineralogical nature of the sample. Here, two distinct constituents can be found (Fig. 7, inset), a coarser fraction of larger (on average) and more translucent quartz grains and a finer fraction of darker magnetite mineral. When sieved into fractions, the optical difference between these two constituents is dramatic, with much of the finer fraction represented by the dark opaque mineral, and much of the larger fraction by the highly translucent quartz grains. Additionally, the differences in reflectance between the two densities increase at the larger phase angles. We explain these findings by the apparent filling of the smaller (and darker fraction) into the voids between the larger and more transparent grains, as the density increases. These filling and compaction effects result in progressive shutdown of the multiple scattering paths of the incident light and added absorption by the darker and more opaque fraction, resulting in the overall dramatic decline in surface reflectance. The reason that this effect is more pronounced at the higher wavelength has to do with the more dominant mineral absorption features in the SWIR range of the spectrum.

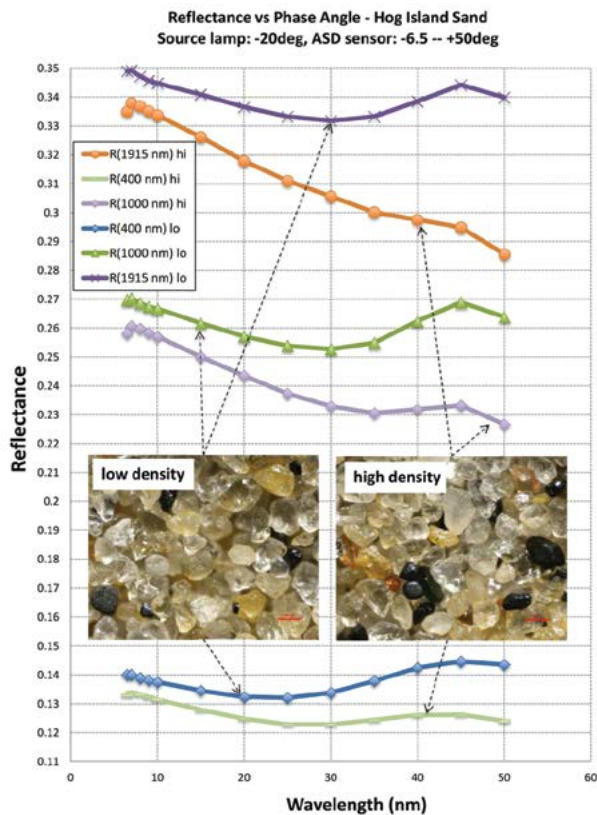


FIGURE 7
 Reflectance of sand samples of low and high relative density at several selected wavelengths. Lower densities display consistently increased reflectance values, especially at higher phase angles, due to mineral complexity, and contrary to current models. Inserts show microscope images (at 4x magnification) of the sand surface at both densities. Note the apparent increase in the darker (and smaller) mineral component at higher relative density.

Conclusions: Thus, we show in this work that if complex beach sands, often a product of many distinct sources of minerals in the coastal zone, contain minerals of distinctly different opacity, they may produce unexpected results in spectral reflectance that are not well characterized or explained by the current models. Moreover, our lab results are reinforced by the field data from other hyperspectral sensors^{4,6,7} collected at the VCR, including the NRL field goniometer hyperspectral tool (near-surface measurement) and the airborne sensors. Another consequence of these findings is that data collected at multiple phase angles in these complex sands may yield information on relative density, and, consequently, estimates of the friction angle of granular media.

[Sponsored by NRL Base Program (CNR funded)]

References

- ¹ B. Hapke, "Bidirectional Reflectance Spectroscopy: 6. Effects of Porosity," *Icarus* **195**(2), 918–926 (2008).
- ² P. Helfenstein and M.K. Shepard, "Testing the Hapke Photometric Model: Improved Inversion and the Porosity Correction," *Icarus* **215**, 83–100 (2011).
- ³ C.M. Bachmann, W. Philpot, A. Abelev, and D. Korwan, "Phase Angle Dependence of Sand Density Observable in Hyperspectral Reflectance," *Remote Sensing of the Environment* (in review).
- ⁴ C.M. Bachmann, A. Abelev, et al., "A Multi-Sensor Approach to Coastal Characterization," in *Optical Remote Sensing of the Environment, Sensor Fusion and Lidar I (RTu1E)* (Optical Society of America, 2012).
- ⁵ J. Kolbuszewski, L. Nadolski, and Z. Dydacki, "Porosity of Wind-deposited Sands," *Geological Magazine* **87**, 433–435 (1950).
- ⁶ C.M. Bachmann, D. Gray, A. Abelev, and W.D. Philpot, "Linking Goniometer Measurements to Hyperspectral and Multi-Sensor Imagery for Retrieval of Beach Properties and Coastal Characterization," in *SPIE Defense, Security, and Sensing: Algorithms, and Technologies for Multispectral, Hyperspectral, and Ultraspectral Imagery XVIII* **8390-48** (2012).
- ⁷ C.M. Bachmann, D. Gray, A. Abelev, et al., "A Field Portable Hyperspectral Goniometer for Coastal Characterization" (*IEEE Geoscience and Remote Sensing Society (GRSS)*, 2012). doi:WEPP.380.